Chaos and graphics

Visualising chaos in a model of brain electrical activity

Mathew P. Dafilis[a], Paul D. Bourke[b], David T.J. Liley[a],*, Peter J. Cadusch[c]

[a] *Centre for Intelligent Systems and Complex Processes, School of Biophysical Sciences and Electrical Engineering, Swinburne University of Technology, PO Box 218, Hawthorn, VIC 3122, Australia*
[b] *Centre for Astrophysics and Supercomputing, School of Biophysical Sciences and Electrical Engineering, Swinburne University of Technology, Hawthorn, VIC, Australia*
[c] *School of Biophysical Sciences and Electrical Engineering, Swinburne University of Technology, Hawthorn, VIC, Australia*

Abstract

It is a major source of contention in brain dynamics as to whether the electrical rhythms of the brain show signs of chaos. Here we discuss evidence for the existence of chaos in a theory of brain electrical activity and provide unique depictions of the dynamics of this model.
© 2002 Elsevier Science Ltd. All rights reserved.

1. Introduction

Perhaps the most often asked question of researchers in brain dynamics over the past decade has been—"is there chaos in the brain?", with this very question the subject of serious experimental investigation over the past few years [1]. However, the development of novel time series analysis techniques and their application to experimentally obtained time series have provided us with overall equivocal results, with many questions still remaining unresolved.

Alongside these experimental endeavours has been the immense corpus of research due to Walter Freeman and colleagues over the past half-century [2]. Based on both his experimental and theoretical studies of the mammalian olfactory system Freeman has suggested that chaos is the very property which allows perception to take place and gives brains the flexibility to rapidly respond in a coherent manner to perceptual stimuli [3].

Freeman's repeated exhortations of the existence of chaos in the brain (as reflected by the existence of chaos in its electrical dynamics) unfortunately has, up until recently, received scant theoretical support, with other existing theories of the electroencephalogram (EEG) either not showing chaos or being unable to do so because of the details of their mathematical construction [4–7].

We have recently shown that chaos exists in Liley's theory of the electroencephalogram [8,9] and that this chaos is widespread and extensive under parametric variation [10]. In this paper we show examples of the chaotic attractors generated by the system and also show an example of the parameter set which supports chaos.

2. The model

The general theory of the electroencephalogram developed by Liley leads to a mathematical model describing the behaviour of two coupled populations of neurones: excitatory (being approximately representative of the pyramidal neurones of neocortex) and inhibitory (being approximately representative of the interneurones of neocortex). The scale of modelling here is approximately that of a cortical macrocolumn, which is a small volume of neocortex containing approximately

*Corresponding author. Tel.: +61-3-9214-8812; fax: +61-9819-0856.
E-mail addresses: pbourke@swin.edu.au (P.D. Bourke), dliley@swin.edu.au (D.T.J. Liley), pcadusch@swin.edu.au (P.J. Cadusch).
URLs: http://astronomy.swin.edu.au/pbourke, http://marr.bsee.swin.edu.au.

10^5 neurones. Each of the two modelled populations is connected to the other population and each population feeds back onto itself in either a mutually excitatory (for the excitatory population) or mutually inhibitory (for the inhibitory population) fashion. Both modelled populations have external excitatory and inhibitory inputs. Inputs to each population, whether from external sources, or from the other population, are modelled based on the dynamics of fast-acting synapses. The mean soma membrane potential of the excitatory population (h_e) is directly related to the local field potential of the neuronal mass, which overwhelmingly dominates the composition of the scalp-recorded electroencephalogram (EEG) [11].

The model equations are:

$$\tau_e \frac{dh_e}{dt} = (h_{er} - h_e) + \frac{h_{eeq} - h_e}{|h_{eeq} - h_{er}|} I_{ee} + \frac{h_{ieq} - h_e}{|h_{ieq} - h_{er}|} I_{ie}, \quad (1)$$

$$\tau_i \frac{dh_i}{dt} = (h_{ir} - h_i) + \frac{h_{eeq} - h_i}{|h_{eeq} - h_{ir}|} I_{ei} + \frac{h_{ieq} - h_i}{|h_{ieq} - h_{ir}|} I_{ii}, \quad (2)$$

$$\frac{d^2 I_{ee}}{dt^2} + 2a \frac{dI_{ee}}{dt} + a^2 I_{ee} = Aae\{N_{ee} S_e(h_e) + p_{ee}\}, \quad (3)$$

$$\frac{d^2 I_{ie}}{dt^2} + 2b \frac{dI_{ie}}{dt} + b^2 I_{ie} = Bbe\{N_{ie} S_i(h_i) + p_{ie}\}, \quad (4)$$

$$\frac{d^2 I_{ei}}{dt^2} + 2a \frac{dI_{ei}}{dt} + a^2 I_{ei} = Aae\{N_{ei} S_e(h_e) + p_{ei}\}, \quad (5)$$

$$\frac{d^2 I_{ii}}{dt^2} + 2b \frac{dI_{ii}}{dt} + b^2 I_{ii} = Bbe\{N_{ii} S_i(h_i) + p_{ii}\}, \quad (6)$$

where

$$S_q(h_q) = q_{\max}/(1 + \exp(-\sqrt{2}(h_q - \theta_q)/s_q)), \quad q = e, i.$$

Eqs. (1) and (2) describe h_e and h_i, the mean soma membrane potentials of the excitatory and inhibitory populations, respectively. Eqs. (3)–(6) describe the effective "synaptic" activity of type j acting upon neurones of type k given by I_{jk}. The S functions represent the conversion of the membrane potential of the respective population into an equivalent mean firing rate. For further manipulation and for numerical solution we rewrite these equations as a set of ten coupled nonlinear first-order ordinary differential equations.

For a complete discussion of the equations and the methods used to solve them, as well as a further discussion about the work we present herein, please see Dafilis et al. [10]. A further discussion of Liley's theory may be found in Liley et al. [9], which includes a detailed derivation of the theory, and a comprehensive discussion of the theory and its predictions. A somewhat abbreviated version is available in Liley et al. [8].

3. Results and visualisations

During the course of our investigations into the dynamical complexity of the model we found solutions which had complicated temporal behaviour including aperiodic oscillations. We surmised that these model solutions were indeed chaotic, and in order to ascertain this we used the algorithm of Christiansen and Rugh [12] to determine the largest Lyapunov exponent for the system. The presence of a positive largest Lyapunov exponent for the system is confirmation of the chaotic nature of the system's behaviour.

Initial representations of the surfaces and the attractors were first determined using locally developed software based on the OpenGL standard, which provided for interactive manipulation of the graphics with respect to orientation and preliminary colourings. Subsequent to the selection of informative orientations and colourings the graphics were prepared for rendering using locally developed software to create the requisite representations. Raytracings were performed using POV-Ray, one of a number of freely available ray tracing packages.

Figs 1 and 2 illustrate two different chaotic attractors from the system for two unique sets of parameters. The attractors shown are created from time series of the h_e variable of the system, as h_e is directly proportional to the electrical activity recorded by electrodes placed on the scalp. Attractors were time delay embedded using an embedding delay corresponding approximately to that of the location of the first zero of the autocorrelation function for each time series. Each time series is 100 s long, with the initial 5 s of the simulation discarded to remove any transient effects. Time series were generated at a resolution of 1 point/ms (yielding a time series of overall length 100,000 points) using the CVODE [13] integrator option of XPPAUT [14] (a dynamical systems simulation package), with time delay embeddings and autocorrelations obtained using software from the TISEAN package [15].

One of the undisputed objectives of effective scientific visualisation is to provide researchers with an enhanced understanding of the dynamics of the processes they are interested in visualising. Researchers typically make use of simple geometries, efficient renderings, and stark colours. In this way, the details of the visualisation process and the myriad opportunities it provides for depicting the data do not obscure and overwhelm the detail of the data to be visualised.

On the other hand, a counterpoint to the above would be to suggest that whilst the purpose of an effective scientific visualisation is to present the data in a way such that the science behind the image is more easily interpreted, an effective visualisation should also look good, and be visually appealing. Empirically one may suggest that making a visualisation more attractive
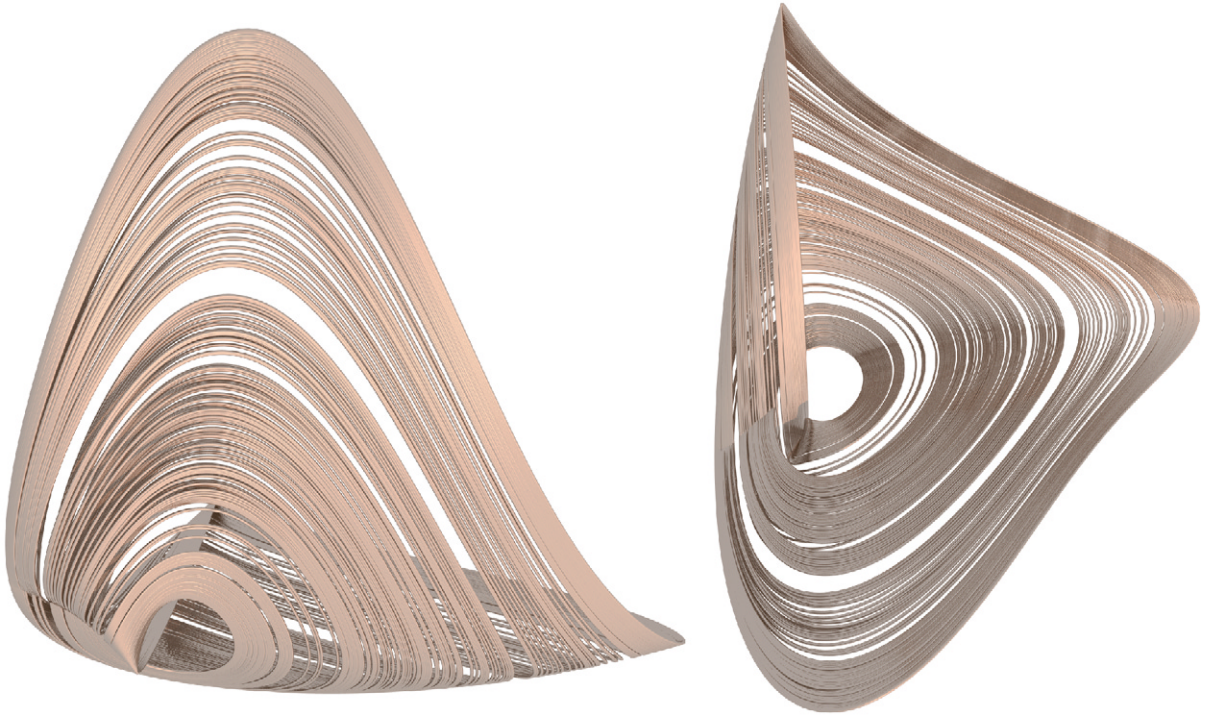
Fig. 1. Two complementary views of a chaotic attractor from the model, shown from two different perspectives. Note the shadowing and how it provides an enhanced sense of the depth of the attractor.
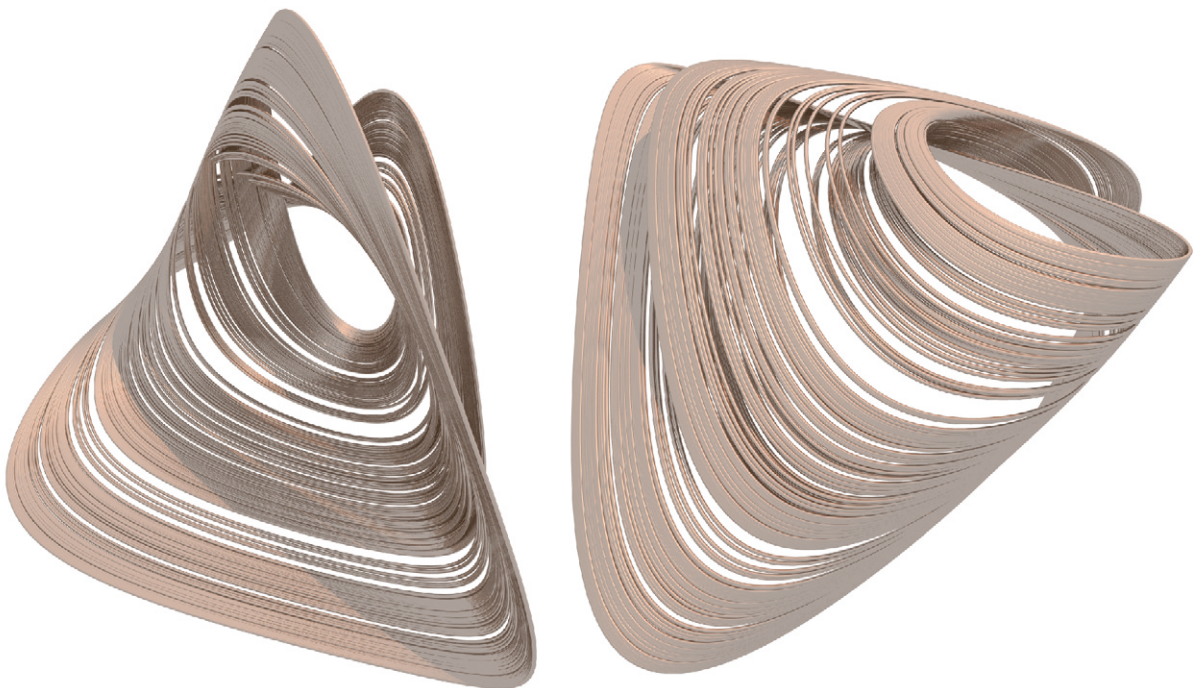

Fig. 2. Two different views of another chaotic attractor. Note how the rendering provides a perspective on the interleaving of the attractor's sheets and folds.
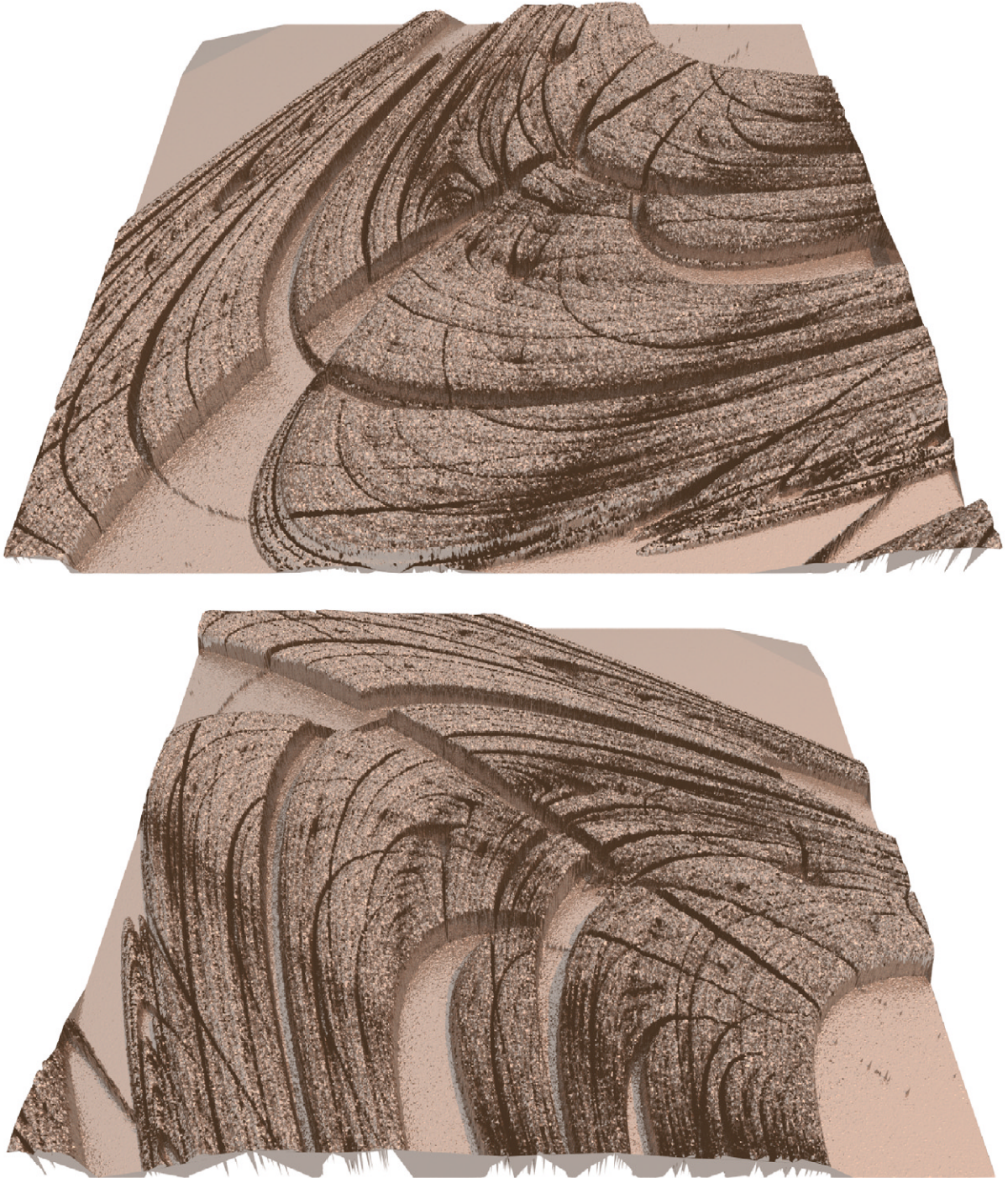
Fig. 3. Two different views of the parameter space plane of the model, with the largest Lyapunov exponent of the system as the dependent variable and the external excitatory input pulse density to the excitatory (p_{ee}) and inhibitory (p_{ei}) populations as the independent variables. Model parameters and bounds: $p_{ee} = 9$–12.25 ms^{-1}, $p_{ei} = 7.5$–10.75 ms^{-1}, $a = 0.49$ ms^{-1}, $b = 0.592$ ms^{-1}, $A = 0.81$ mV, $B = 4.85$ mV, $e_{\max} = i_{\max} = 0.5$ ms^{-1}, $h_{eeq} = 45$ mV, $h_{er} = h_{ir} = -70$ mV, $h_{ieq} = -90$ mV, $N_{ee} = N_{ei} = 3034$, $N_{ie} = N_{ii} = 536$, $p_{ie} = p_{ii} = 0$ ms^{-1}, $s_e = s_i = 5$ mV, $\theta_e = \theta_i = -50$ mV, $\tau_e = 9$ ms, $\tau_i = 39$ ms. Choosing a (p_{ee}, p_{ei}) pair from within this plane, along with the specified parameter set, and numerically solving the model equations, will lead to a variety of different attractors, from point attractor to limit cycle to chaotic. Values of p_{ee} and p_{ei} outside of the bounds indicated above will also lead to chaos—for a depiction of the complete parameter space which supports chaos for this parameter set, see [10].

makes it more pleasant, and perhaps, easier to look at, so the researcher may find it much easier to appreciate and understand the visualisation and implicitly the science underpinning the image.

It is primarily for these reasons that we have chosen relatively sparse colour schemes and straightforward raytracings—these selections make the data more attractive and visually appealing, as well as enabling greater insight into the overall structure of the data. This is best illustrated by considering the effect the raytracing provides by placing shadows on the attractor surfaces. The shadows help to better represent the spatial extent and dimension of the objects in the three-dimensional space in which they are situated, with the uniform, pale colourings helping to maintain a clear distinction between the representation of the shadows and the representation of the surface itself.

Each of the attractors has only one positive Lyapunov exponent; it follows via the Kaplan–Yorke conjecture [16] that the dimension of each of these attractors is therefore larger than 2 but less than 3. Note how the rendering provides a clear definition of the perspective and shadowing of the model. This adds considerably to an appreciation of how complicated the attractors, and therefore the dynamics of the system are for different sets of model parameters.

Fig. 3 complements Figs 1 and 2 by providing a qualitative description of the dynamics of the model under parametric variation of the two of the most important model parameters: the external excitatory pulse densities to the excitatory (p_{ee}) and inhibitory (p_{ei}) neural model populations.

At many hundreds of thousands of locations in the plane, we determined the largest Lyapunov exponent of the system to determine whether the dynamics of the system are chaotic for that particular combination of p_{ee} and p_{ei}. As mentioned earlier, chaotic dynamics have a positive largest Lyapunov exponent (LLE). Limit cycle dynamics have a LLE of zero, and point attractor dynamics have a LLE which is negative. The height of the plane at a particular point is given by the LLE of the attractor at that point.

The flat region of the plane is where limit cycle dynamics are found. The elevated regions of the plane, with their characteristic puckered and wrinkled appearance, are where chaotic dynamics, like that shown in Figs 1 and 2, arise in parameter space.

It is evident that, to some degree, the distribution of chaotic dynamics in this parameter space has some self-similarity, and that it is solid in parameter space. We have shown that chaos within this parameter space has structure consistent with that of a *fat fractal*, which is an object with structure at all scales which has positive measure.

Note how the relatively neutral colour palette and the judicious use of light sources and their positioning allows the nuances and the fine details of the distribution of heights in the plane to be drawn out, without obscuring the limit cycle regions of the plane or casting inappropriate shadows.

This rendering, with its homogeneous palette, is not able to clearly differentiate to the viewer the diversity of the "heights" in the plane, as would a colouring where the colour at each point is proportional to the point's effective height. Such an image would essentially be two-dimensional, with the colouring at each location representative of the third dimension. We consider Fig. 3 to be complementary to such a depiction and not in direct competition with such a depiction. Fig. 3 provides a much better understanding of the structure of the parameter space region as opposed to a coloured representation, as this representation allows one to focus on how the dynamics are structured without having the obscuring effect of having to interpret the colour of the image at each location. Arguably the three-dimensional representation of the data set gives an enhanced aesthetic which makes interpreting and understanding the structure of chaos within the parameter space less difficult. The complexity of the structure within this plane is without question, as are its fat fractal characteristics.

4. Conclusion

We have presented evidence for complicated dynamics in a model of brain electrical activity and further have illustrated these dynamics using a novel method.

It is evident that an appreciation of the dynamics of the model are considerably enhanced by a judicious choice of colour scheme and rendering method, and that, with the right choices, a depiction of the dynamics can be made which is not only aesthetically pleasing but also visually informative.

Acknowledgements

References

[1] Pritchard WS, Duke DW. Measuring "Chaos" in the brain: a tutorial review of EEG dimension estimation. Brain Cognitions 1995;27:353–97.

[2] Freeman WJ. Tutorial on neurobiology: from single neurons to brain chaos. International Journal of Bifurcation and Chaos Applied Science and Engineering 1992;2(3):451–82.

[3] Freeman WJ. The physiology of perception. Scientific American 1991;264(2):78–85.

[4] Zhadin MN. Rhythmic processes in the cerebral cortex. Journal of Theoretical Biology 1984;108:565–95.

[5] Nunez PL. Toward a quantitative description of large-scale neocortical dynamic function and EEG. Behavioural and Brain Science 2000;23:371–437.

[6] Robinson PA, Rennie CJ, Wright JJ. Propagation and stability of waves of electrical activity in the cerebral cortex. Physical Review E 1997;56(1):826–40.

[7] van Rotterdam A, Lopes da Silva FH, van den Ende J, Viergever MA, Hermans AJ. A model of the spatial-temporal characteristics of the alpha rhythm. Bulletin of Mathematical Biology 1982;44(2):283–305.

[8] Liley DTJ, Cadusch PJ, Wright JJ. A continuum theory of electro-cortical activity. Neurocomputing 1999;26–27: 795–800.

[9] Liley DTJ, Cadusch PJ, Dafilis MP. A spatially continuous mean field theory of electrocortical activity.

[10] Dafilis MP, Liley DTJ, Cadusch PJ. Robust chaos in a model of the electroencephalogram: implications for brain dynamics. Chaos 2001;11(3):474–8.

[11] Nunez PL. Electric fields of the brain: the neurophysics of EEG. New York: Oxford University Press, 1981.

[12] Christiansen F, Rugh HH. Computing Lyapunov spectra with continuous Gram-Schmidt orthonormalization. Nonlinearity 1997;10:1063–72.

[13] Cohen SD, Hindmarsh AC. CVODE, a stiff/nonstiff ODE solver in C. Computational Physics 1996;10(2): 138–43.

[14] Ermentrout GB. XPPAUT. URL: http://www.pitt.edu/~phase/

[15] Hegger R, Kantz H, Schreiber T. Practical implementation of nonlinear time series methods: the TISEAN package. Chaos 1999;9(2):413–35.

[16] Kaplan JL, Yorke JA. Chaotic behavior of multidimensional difference equations. In: Peitgen H, Walther H, editors. Functional differential equations and approximation of fixed points. Berlin: Springer, 1979. p. 204–27.

Network: Computation in Neural Systems 2002;13(1): 67–113.